Geochemical Perspectives Letters

An isotopically light nitrogen reservoir in the ocean: evidence from ferromanganese crusts

E.E. Stüeken[1*], M. Bau[2]

OPEN ACCESS

https://doi.org/10.7185/geochemlet.2308

Abstract

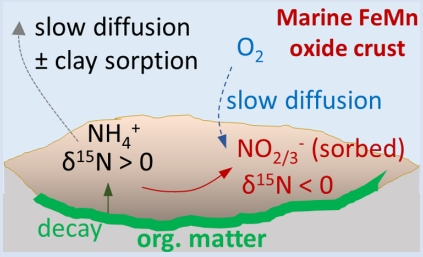

Ferromanganese (FeMn) oxide crusts and nodules in the deep ocean have been studied extensively in the context of critical metals and metal isotope mass balances; however, their role in the marine nitrogen cycle has been unexplored. Here we investigated a suite of hydrogenetic and diagenetic marine FeMn crusts and nodules from the Pacific to determine their isotopic signature and contribution as another N sink from the modern ocean. Our results reveal unusually low $\delta^{15}N$ values down to −12 ‰ in some hydrogenetic crusts, paired with low $\delta^{13}C$ values in carbonate associated with these crusts and nodules. This pattern is most parsimoniously explained by partial oxidation of ammonium (nitrification) derived from benthic biomass. Nitrification generates isotopically light nitrite, which may adhere to FeMn oxides by adsorption. In contrast, the diagenetic and hydrogenetic nodules are enriched in $^{15}N/^{14}N$ to up to +12 ‰, likely due to retention of ammonium in phyllosilicate minerals. Overall, we conclude that FeMn oxide crusts and nodules are a novel archive of microbial activity that may be preserved in the sedimentary record on Earth and possibly Mars.

Received 25 October 2022 | Accepted 14 February 2023 | Published 15 March 2023

Introduction

Ferromanganese (FeMn) oxide deposits in the deep ocean have received increasing attention over the past two decades as they have become recognised as reservoirs of critical metals with potentially economic value (Hein *et al.*, 2000; Lusty *et al.*, 2018). There are three "end member types" of marine FeMn oxide deposits: hydrogenetic crusts and nodules that form very slowly (at a rate of only a few mm/Myr) on exposed rock surfaces at the sediment-water interface; diagenetic nodules that form from pore waters within marine sediments around a nucleus such as a rock fragment; and hydrothermal precipitates that may form as plume fallout or within the sediment (*e.g.*, Koschinsky and Hein, 2017, and references therein). Rare earths and yttrium (REY) concentrations and REY patterns can be used to discriminate between these three genetic pathways, which further attests to their distinct fluid sources, growth rates, and formation mechanisms (Bau *et al.*, 2014). One potentially important factor in the formation of these deposits may be microbial activity, but its role is still unclear. Manganese oxidisers have been detected with genomic techniques (Shiraishi *et al.*, 2016). The presence of biomass within the FeMn oxides therefore opens the possibility of investigating these deposits as novel archives of nitrogen in the sedimentary record. So far, most studies of nitrogen isotopes and abundances in marine sediments have focused on mudrocks (Ader *et al.*, 2016). To our knowledge, FeMn oxides have not previously been studied as geological N repositories. To fill this gap, we selected a suite of hydrogenetic and diagenetic FeMn crusts and nodules from the northern, eastern and southern Central Pacific and three hydrogenetic and mixed type hydrogenetic-diagenetic FeMn nodule certified reference materials from the Atlantic and Pacific (see Supplementary Information for a detailed description of the methods employed). Classification as hydrogenetic *versus* diagenetic is based on the REY concentration and distribution, following the approach outlined in detail by Bau *et al.* (2014). For further discussion of some of these samples see also Bau *et al.* (1996), Schier *et al.* (2021) and Ernst *et al.* (2022).

Results

We find that FeMn oxide nodules, both diagenetic and hydrogenetic, tend to be enriched in total nitrogen (TN) content by a factor of 2.3 on average and display heavier bulk $\delta^{15}N$ values (+3 ‰ to +12 ‰) compared to the hydrogenetic crusts (−12 ‰ to +3 ‰) (Table S-1, Fig. 1a). In contrast, the hydrogenetic crusts are enriched in total inorganic carbon (TIC) by a mean factor of 2.6 (Fig. 1b). Total organic carbon (TOC) does not vary systematically between crusts and nodules (Fig. 1c), but the hydrogenetic crusts express relatively lower organic carbon isotope values ($\delta^{13}C_{org} = -27.8 \pm 0.6$ ‰ *versus* -22.6 ± 2.0 ‰) (Fig. 2a). Carbonate carbon isotopes ($\delta^{13}C_{carb}$) do not vary systematically, but all samples fall below −8 ‰ and are thus depleted relative to open marine carbonate which falls near 0 ‰ (Fig. 2b). Our results for the certified reference materials NOD-P1, NOD-A1 and JMn-1 fall within the respective range observed for the other samples (Fig. 1a).

1. School of Earth and Environmental Sciences, University of St Andrews, Bute Building, Queen's Terrace, St Andrews, Fife, KY16 9TS, United Kingdom
2. CritMET – Critical Metals for Enabling Technologies, School of Science, Constructor University, Campus Ring 1, 28759 Bremen, Germany
* Corresponding author (email: ees4@st-andrews.ac.uk)

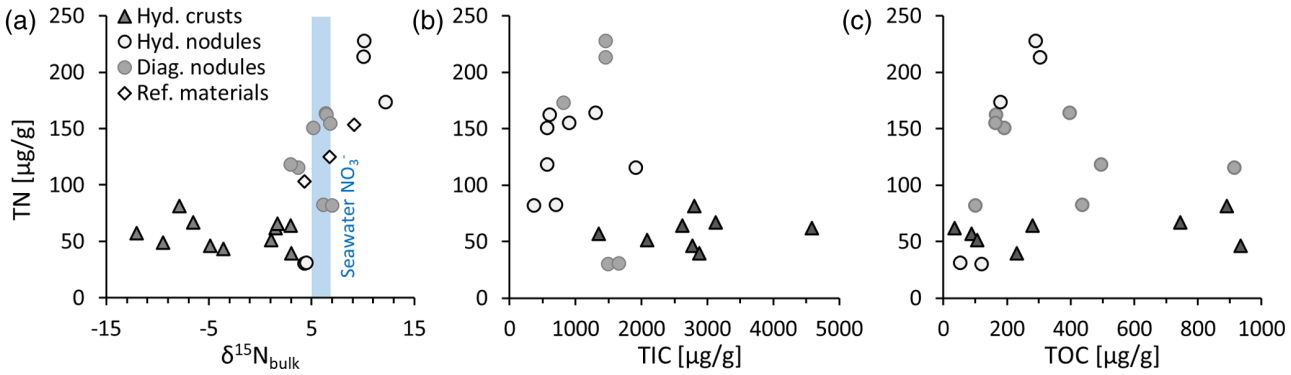

Figure 1 **(a)** Total nitrogen (TN) *versus* $\delta^{15}N_{bulk}$. **(b)** TN *versus* total inorganic carbon (TIC). **(c)** TN *versus* total organic carbon (TOC). The hydrogenetic crusts are relatively depleted in $\delta^{15}N_{bulk}$ and TN but enriched in TIC.

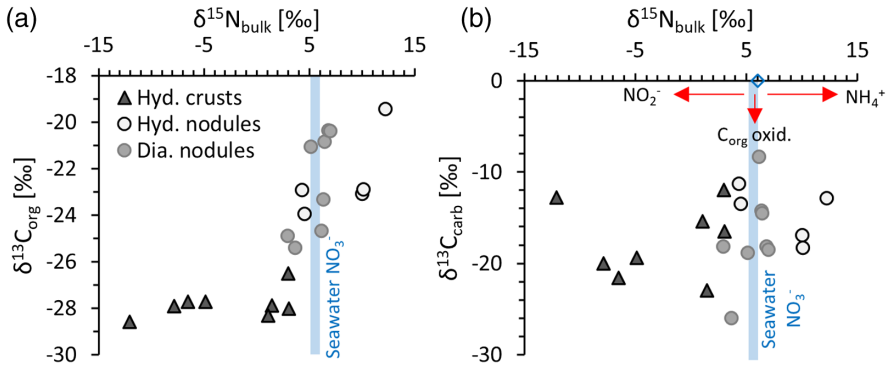

Figure 2 **(a)** $\delta^{13}C_{org}$ *versus* $\delta^{15}N_{bulk}$. **(b)** $\delta^{13}C_{carb}$ *versus* $\delta^{15}N_{bulk}$. The hydrogenetic crusts tend to be depleted in $\delta^{15}N_{bulk}$ relative to average seawater (blue line), possibly reflecting intake of isotopically light NO_2^- generated within sediments from NH_4^+ oxidation. Slight enrichment in $\delta^{15}N_{bulk}$ in diagenetic oxides may reflect retention of isotopically heavy NH_4^+ after partial oxidation.

Discussion

The nitrogen isotopic composition of some of the hydrogenetic crusts is unusually depleted in ^{15}N. For comparison, average marine mud from the modern ocean clusters around a mean of +5 ‰ to +6 ‰ (Tesdal *et al.*, 2013), which reflects the isotopic composition of seawater nitrate – the major nitrogen source for algae that is captured in sediments *via* biomass burial. However, values in the negative range are rare throughout the siliciclastic rock record (Ader *et al.*, 2016). There are four possible mechanisms that could explain such low $\delta^{15}N$ values:

(1) *Biological nitrogen fixation by alternative nitrogenases*. When dissolved N becomes biologically limiting, some microbes are able to convert N_2 into ammonium, a process known as nitrogen fixation that is catalysed by the enzyme nitrogenase. Most nitrogenases contain Mo at a catalytic centre, and those impart an isotopic fractionation ($\varepsilon = \delta^{15}N_{reactant} - \delta^{15}N_{product}$) of 1–2 ‰ on the resulting biomass. Under Mo-depleted conditions, V or Fe can be used instead, and these so called alternative nitrogenases impart larger fractionations of up to 8 ‰ (Zhang *et al.*, 2014). However, it is unlikely that this metabolism caused the low $\delta^{15}N$ values in our samples, because the deep ocean is enriched in both nitrate and Mo, meaning that nitrogen fixation is not required, and, if necessary, the more efficient Mo-based nitrogenase would likely be preferred.

(2) *Dissimilatory nitrate reduction to ammonium (DNRA)*. Given the high abundance of nitrate in the deep ocean with an isotopic composition of around +5 ‰ to +6 ‰, it is conceivable that the low $\delta^{15}N$ values reflect ammonium generated by DNRA, which imparts a fractionation of up to 30 ‰ (McCready *et al.*, 1983). However, this metabolism is unlikely to take place within an environment where Mn(IV) oxides are thermodynamically stable, because Mn has a high redox potential that is not compatible with nitrate reduction (Brookins, 1988).

(3) *Partial assimilation of either ammonium or nitrate into biomass*. It has been suggested that FeMn crusts are populated by microorganisms (*e.g.*, Kato *et al.*, 2019), and these could be fractionating $^{15}N/^{14}N$ ratios as they uptake nitrate ($\varepsilon = 5$–10‰) or ammonium ($\varepsilon = 14$–27‰) into their biomass (Casciotti, 2009). Nitrate is readily available in seawater (30 µM on average; *e.g.*, Webb, 2021), and ammonium could potentially be supplied by decaying biomass underneath or within the FeMn crust. Both would likely have a starting composition of +5 ‰ to +6 ‰, as observed for marine nitrate and average marine sediments (Tesdal *et al.*, 2013). Hence this mechanism offers a plausible explanation for the $\delta^{15}N$ data; however, it does not account for the light $\delta^{13}C_{carb}$ values in the same samples.

(4) *Partial oxidation of ammonium (nitrification) to nitrite and nitrate*. In the oxidising environment of the FeMn crusts, ammonium would likely undergo oxidation. This microbially catalysed reaction produces isotopically light nitrite and later nitrate in a second step, while the residual ammonium becomes enriched in ^{15}N (Fig. 3). If the oxidation process does not go to completion, perhaps due to diffusion limited O_2 migration into the crusts as described in sediments elsewhere (Morales *et al.*, 2014), isotopically light nitrite/nitrate may accumulate and become incorporated into the crust, either by uptake into fresh biomass or by adsorption to the mineral surface (as documented for nitrate by Takematsu *et al.*, 1990). This could plausibly explain the $\delta^{15}N$ values of the hydrogenetic crusts. Indeed, nitrifying

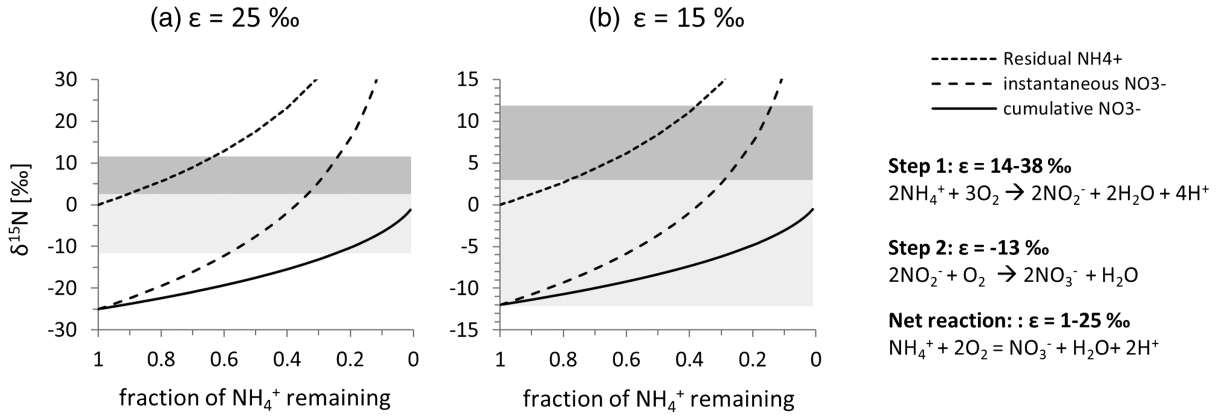

Figure 3 Proposed mechanism of partial NH^{4+} oxidation to NO_3^- *via* NO_2^- and associated Rayleigh fractionation. **(a)** Fractionation ($\varepsilon = \delta^{15}N_{reactant} - \delta^{15}N_{product}$) of 25 ‰, maximum net fractionation for $NH_4^+ \rightarrow NO_3^-$. **(b)** Fractionation of 15 ‰, smallest possible fractionation to explain the data. Reactions on the right show that partial oxidation could also generate light NO_2^-. Light grey shading = range of $\delta^{15}N$ values seen in hydrogenetic crusts; dark grey shading = range of $\delta^{15}N$ values seen in diagenetic and hydrogenetic nodules.

organisms of the phylum *Thaumarchaea* have been documented by molecular techniques from several deep marine FeMn oxides (*e.g.*, Kato *et al.*, 2019; Bergo *et al.*, 2021).

It has been suggested that these nitrifying organisms are feeding on trace levels of ammonium dissolved in the deep ocean (Wuchter *et al.*, 2006; Kato *et al.*, 2019). While this appears possible, it would, however, leave the light $\delta^{13}C_{carb}$ values unexplained. Such light $\delta^{13}C_{carb}$ values most likely reflect *in situ* oxidation of organic matter to dissolved inorganic carbon (DIC) within pore waters. This diagenetic DIC pool would inherit the isotopic composition of local biomass (<−20 ‰, Fig. 2a), such that variable mixing with seawater ($\delta^{13}C \approx 0$ ‰) can explain the observed $\delta^{13}C_{carb}$ values between −28 ‰ and −8 ‰ (Fig. 2b). The carbon isotope data are thus evidence for degradation of older biomass from within the FeMn oxides. This biomass is the most likely source of ammonium for nitrification, because the Redfield ratio of average marine organisms dictates that 1 mole of N is released for every 7–10 mole of organic C (Godfrey and Glass, 2011). We note that $\delta^{15}N_{bulk}$ and $\delta^{13}C_{carb}$ are not directly correlated, but as the isotopically light N and C are likely associated with different minerals and undergo variable mixing with isotopically heavier phases, a correlation cannot necessarily be expected.

Overall, the most plausible scenario for the N-C isotope systematics observed in the hydrogenetic FeMn crusts is, therefore, the presence of a benthic biosphere, where older biomass underwent oxidation and nitrification, catalysed by active organisms. Some of the products (including isotopically light nitrite/nitrate) were re-assimilated into fresh biomass and/or adsorbed to mineral surfaces, while the oxidised organic carbon was partly redeposited as carbonate. This interpretation is consistent with biomolecular evidence of nitrifiers from FeMn crusts worldwide (see above). However, it leaves open the question as to what happened to the residual isotopically heavy ammonium. We speculate that in the case of the isotopically lightest hydrogenetic FeMn crusts this ammonium was diffusively lost to the water column. This may indicate that the preferential retention of nitrite/nitrate within the FeMn crust was driven by adsorption rather than biological uptake, because the latter would typically prefer ammonium. Nitrite adsorption on FeMn oxides has to our knowledge not been studied systematically, but we note that empirical data from one study suggest concentrations of around 50 $\mu g \cdot g^{-1}$ of nitrate at equilibrium with seawater (Takematsu *et al.*, 1990), which is consistent with our data.

In the case of the diagenetic and hydrogenetic nodules, we also see low $\delta^{13}C_{carb}$ values indicative of biomass oxidation; however, $\delta^{15}N$ shows no evidence of light nitrite/nitrate retention. Instead, $\delta^{15}N$ values of up to 12 ‰ and comparatively high TN abundances may indicate that isotopically heavy ammonium (*i.e.* the residuum after partial nitrification) was preferentially retained (Fig. 3), possibly due to a higher clay or active biomass content within these samples. Ammonium (NH_4^+) has a similar ionic radius to K^+, which allows it to substitute into potassic phyllosilicates during diagenesis (Müller, 1977). Retention of isotopically heavy ammonium in the clay matrix would probably have overwhelmed the proportion of adsorbed isotopically light nitrite/nitrate, such that the bulk average $\delta^{15}N$ value of the nodular samples is positive. Further work is needed to test this hypothesis. We also note the systematically higher $\delta^{13}C_{org}$ values within nodules compared to crusts (Fig. 3a), which likely point towards an ecosystem with different carbon fixation pathways. This interpretation is broadly consistent with a distinct microenvironment with differing nutrient inventories.

Conclusions

In summary, our data reveal novel insights into biological processes that take place within FeMn oxide deposits in the deep sea, including biological oxidation of biomass *in situ*, which led to the formation of isotopically light DIC and nitrite/nitrate (Figs. 3, 4). The latter may be trapped by adsorption to oxide minerals. Our results thus uncover a mechanism for generating a previously unknown repository of isotopically light nitrogen in marine sediments. However, it is unlikely that this repository contributes significantly to the global mass balance of N burial from the ocean. For example, assuming a global average mass accumulation rate of 24.8×10^9 g for FeMn oxides in the deep ocean (*e.g.*, Ernst *et al.*, 2022) with an average concentration of TN of 57 ± 12 $\mu g \cdot g^{-1}$ (Table S-1) would lead to a N burial flux of $1.4 \cdot 10^6$ $g \cdot yr^{-1}$. For comparison, the amount of N buried in siliciclastic marine sediments globally with a mean concentration of 560 ± 230 $\mu g \cdot g^{-1}$ (Johnson and Goldblatt, 2015) at a sedimentation rate of 10^{16} $g \cdot yr^{-1}$ (Gregor, 1985) yields an N burial flux of $5.6 \cdot 10^{12}$ $g \cdot yr^{-1}$ and thus dominates as the major sink. However, our study uncovers a novel archive of microbial activity that may be preserved in the rock record and contribute reconstructions of biological

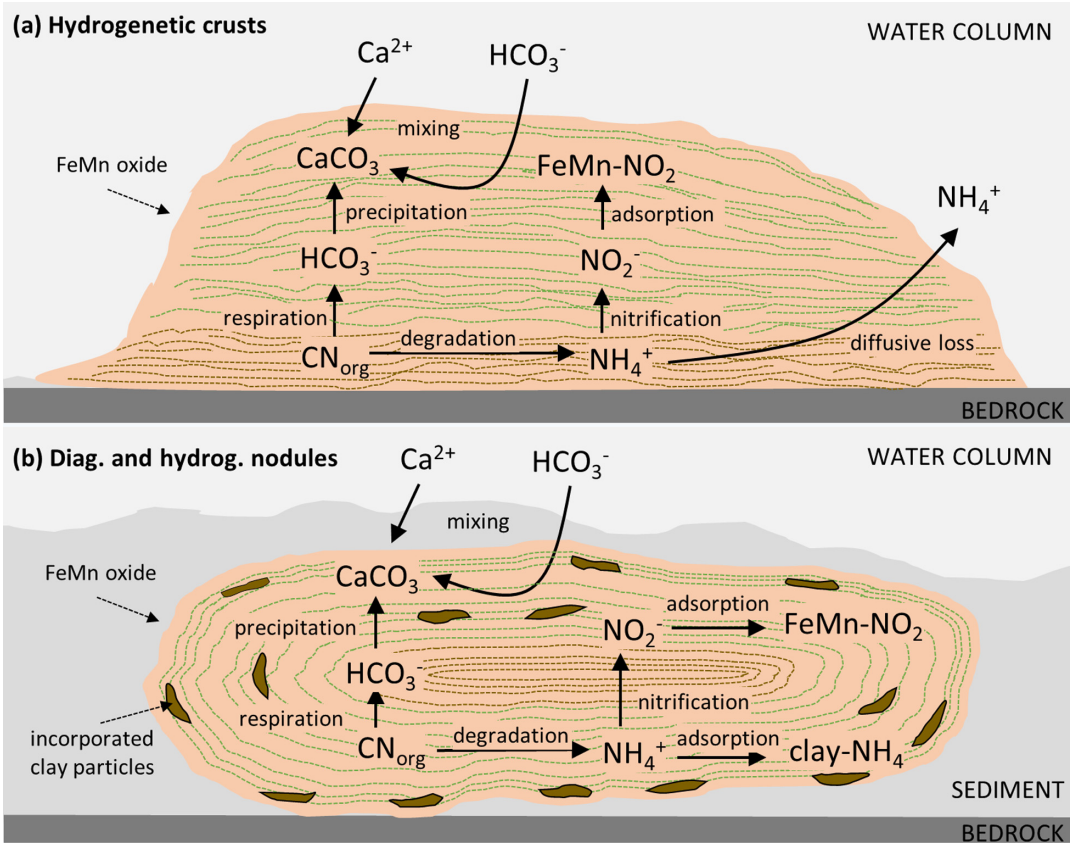

Figure 4 Environmental sketch. Dead biomass (dotted brown lines) releases ammonium during degradation, which is partially oxidised to nitrite. Some of this nitrite is trapped in FeMn oxides by adsorption and possibly by assimilation into fresh biomass (dotted pale green lines). **(a)** In hydrogenetic crusts, the residual ^{15}N-enriched ammonium is lost to the water column by diffusion. **(b)** In diagenetic and hydrogenetic nodules, some of the ammonium is retained in clay minerals, leading to higher bulk δ^{15}N values and TN abundances.

evolution over Earth history, or serve as a biosignature in Martian settings.

Acknowledgements

EES acknowledges funding from a NERC Frontiers grant (NE/V010824/1). MB acknowledges funding from Deutsche Forschungsgemeinschaft (DFG SPP1833 grant BA-2289/8-1). We thank Claudine Stirling for editorial handling and two anonymous reviewers for constructive feedback that improved the manuscript.

Editor: Claudine Stirling

Additional Information

Supplementary Information accompanies this letter at https://www.geochemicalperspectivesletters.org/article2308.

Cite this letter as: Stüeken, E.E., Bau, M. (2023) An isotopically light nitrogen reservoir in the ocean: evidence from ferromanganese crusts. *Geochem. Persp. Let.* 25, 13–17. https://doi.org/10.7185/geochemlet.2308

References

Ader, M., Thomazo, C., Sansjofre, P., Busigny, V., Papineau, D., Laffont, R., Cartigny, P., Halverson, G.P. (2016) Interpretation of the nitrogen isotopic composition of Precambrian sedimentary rocks: Assumptions and perspectives. *Chemical Geology* 429, 93–110. https://doi.org/10.1016/j.chemgeo.2016.02.010

Bau, M., Koschinsky, A., Dulski, P., Hein, J.R. (1996) Comparison of the partitioning behaviours of yttrium, rare earth elements, and titanium between hydrogenetic marine ferromanganese crusts and seawater. *Geochimica et Cosmochimica Acta* 60, 1709–1725. https://doi.org/10.1016/0016-7037(96)00063-4

Bau, M., Schmidt, K., Koschinsky, A., Hein, J., Kuhn, T., Usui, A. (2014) Discriminating between different genetic types of marine ferro-manganese crusts and nodules based on rare earth elements and yttrium. *Chemical Geology* 381, 1–9. https://doi.org/10.1016/j.chemgeo.2014.05.004

Bergo, N.M., Bendia, A.G., Ferreira, J.C.N., Murton, B.J., Brandini, F.P., Pellizari, V.H. (2021) Microbial diversity of deep-sea ferromanganese crust field in the Rio Grande Rise, Southwestern Atlantic Ocean. *Microbial Ecology* 82, 344–355. https://doi.org/10.1007/s00248-020-01670-y

Brookins, D.G. (1988) *Eh-pH Diagrams for Geochemistry*, Springer-Verlag, New York. https://doi.org/10.1007/978-3-642-73093-1

Casciotti, K.L. (2009) Inverse kinetic isotope fractionation during bacterial nitrite oxidation. *Geochimica et Cosmochimica Acta* 73, 2061–2076. https://doi.org/10.1016/j.gca.2008.12.022

Ernst, D.M., Schier, K., Garbe-Schönberg, D., Bau, M. (2022) Fractionation of germanium and silicon during scavenging from seawater by marine Fe (oxy) hydroxides: Evidence from hydrogenetic ferromanganese crusts and nodules. *Chemical Geology* 595, https://doi.org/10.1016/j.chemgeo.2022.120791

Godfrey, L.V., Glass, J.B. (2011) The geochemical record of the ancient nitrogen cycle, nitrogen isotopes, and metal cofactors. *Methods in Enzymology* 486, 483–506. https://doi.org/10.1016/B978-0-12-381294-0.00022-5

Gregor, C.B. (1985) The mass-age distribution of Phanerozoic sediments. In: Snelling, N.J. (Ed.) *The chronology of the geologic record*. The Geological Society of London, London, UK, 284–289. https://doi.org/10.1144/GSL.MEM.1985.010.01.22

Hein, J.R., Koschinsky, A., Bau, M., Manheim, T., Kang, J.-K., Roberts, L. (2000) Cobalt rich ferromanganese crusts in the Pacific. In: Cronan, D.S. (Ed.) *Handbook of Marine Mineral Deposits*. CRC Press, Boca Raon, Florida, 239–279. https://doi.org/10.1201/9780203752760-9

Johnson, B., Goldblatt, C. (2015) The Nitrogen budget of Earth. *Earth-Science Reviews* 148, 150–173. https://doi.org/10.1016/j.earscirev.2015.05.006

Kato, S., Hirai, M., Ohkuma, M., Suzuki, K. (2019) Microbial metabolisms in an abyssal ferromanganese crust from the Takuyo-Daigo Seamount as revealed by metagenomics. *PLoS ONE* 14, p.e0224888. https://doi.org/10.1371/journal.pone.0224888

Koschinsky, A., Hein, J.R. (2017) Marine ferromanganese encrustations: archives of changing oceans. *Elements* 13, 177–182. https://doi.org/10.2113/gselements.13.3.177

Lusty, P.A., Hein, J.R., Josso, P. (2018) Formation and occurrence of ferromanganese crusts: earth's storehouse for critical metals. *Elements* 14, 313–318. https://doi.org/10.2138/gselements.14.5.313

McCready, R.G.L., Gould, W.D., Barendregt, R.W. (1983) Nitrogen isotope fractionation during the reduction of NO_3^- to NH_4^+ by Desulfovibrio sp. *Canadian Journal of Microbiology* 29, 231–234. https://doi.org/10.1139/m83-038

Morales, L.V., Granger, J., Chang, B.X., Prokopenko, M.G., Plessen, B., Gradinger, R., Sigman, D.M. (2014) Elevated $^{15}N/^{14}N$ in particulate organic matter, zooplankton, and diatom frustule-bound nitrogen in the ice-covered water column of the Bering Sea eastern shelf. *Deep Sea Research Part II: Topical Studies in Oceanography* 109, 100–111. https://doi.org/10.1016/j.dsr2.2014.05.008

Müller, P.J. (1977) CN ratios in Pacific deep-sea sediments: Effect of inorganic ammonium and organic nitrogen compounds sorbed by clays. *Geochimica et Cosmochimica Acta* 41, 765–776. https://doi.org/10.1016/0016-7037(77)90047-3

Schier, K., Ernst, D.M., de Sousa, I.M.C., Garbe-Schönberg, D., Kuhn, T., Hein, J.R., Bau, M. (2021) Gallium-aluminum systematics of marine hydrogenetic ferromanganese crusts: Inter-oceanic differences and fractionation during scavenging. *Geochimica et Cosmochimica Acta* 310, 187–204. https://doi.org/10.1016/j.gca.2021.05.019

Shiraishi, F., Mitsunobu, S., Suzuki, K., Hoshino, T., Morono, Y., Inagaki, F. (2016) Dense microbial community on a ferromanganese nodule from the ultra-oligotrophic South Pacific Gyre: Implications for biogeochemical cycles. *Earth and Planetary Science Letters* 447, 10–20. https://doi.org/10.1016/j.epsl.2016.04.021

Takematsu, N., Sato, Y., Okabe, S., Usui, A. (1990) Uptake of selenium and other oxyanionic elements in marine ferromanganese concretions of different origins. *Marine Chemistry* 31, 271–283. https://doi.org/10.1016/0304-4203(90)90042-B

Tesdal, J.E., Galbraith, E.D., Kienast, M. (2013) Nitrogen isotopes in bulk marine sediment: linking seafloor observations with subseafloor records. *Biogeosciences* 10, 101–118. https://doi.org/10.5194/bg-10-101-2013

Webb, P. (2021) *Introduction to Oceanography*, Pressbooks. Rebus Community: Montreal, QC, Canada, 393pp.

Wuchter, C., Abbas, B., Coolen, M.J., Herfort, L., van Bleijswijk, J., Timmers, P., Strous, M., Teira, E., Herndl, G.J., Middelburg, J.J., Schouten, S. (2006) Archaeal nitrification in the ocean. *Proceedings of the National Academy of Sciences* 103, 12317–12322. https://doi.org/10.1073/pnas.0600756103

Zhang, X., Sigman, D.M., Morel, F.M., Kraepiel, A.M. (2014) Nitrogen isotope fractionation by alternative nitrogenases and past ocean anoxia. *Proceedings of the National Academy of Sciences* 111, 4782–4787. https://doi.org/10.1073/pnas.1402976111

Geochemical Perspectives Letters

An isotopically light nitrogen reservoir in the ocean: evidence from ferromanganese crusts

E.E. Stüeken, M. Bau

Supplementary Information

The Supplementary Information includes:

- Analytical methods
- Figure S-1
- Table S-1
- Supplementary Information References

Analytical methods

The samples were analysed in bulk and after acid treatment, using facilities in the St Andrews Isotope Geochemistry Laboratories (StAIG) (e.g., Stüeken *et al.*, 2020). For the acid treatment, approximately 0.5-1 g of rock powder were weighed into pre-combusted glass centrifuge tubes (500 °C for 2 hours) and mixed with 10 ml of 2N HCl (reagent grade). The tubes were capped loosely to allow escape of CO_2 gas. The acid was left to react overnight at 70 °C in a closed oven and decanted the next day after centrifugation (700 rpm for 15 minutes). The residues were washed three times with 18.2 MΩ·cm^{-1} and then left to dry in the oven for two days before transfer into pre-combusted scintillation vials. For determination of carbon and nitrogen abundances and isotopic ratios in acid-treated residues and in bulk rocks, the powders were weighed into tin capsules and analysed by flash combustion in an elemental analyser (EA Isolink) coupled to an isotope-ratio mass spectrometer (MAT253) via a Conflo IV (all Thermo Fisher). The EA was operated in dual-reactor mode, where the first reactor was packed with Cr_2O_3 and silvered cobaltic cobaltous oxide at 1020 °C for complete combustion and sulphur removal, respectively, while the second reactor was packed with Cu wire at 650 °C for conversion of nitrogen oxides into N_2 gas. A magnesium perchlorate column at room temperature was used to remove water from the gas stream. The gas chromatograph column of the EA was ramped from 35 °C

to 240 °C during each analysis to optimize elution of CO_2. The standards USGS-40 and USGS-41 were used to calibrate the data to standard delta notation (δ [‰] = [$R_{sample}/R_{standard} - 1$] x 1000), where R = $^{13}C/^{12}C$ for $\delta^{13}C$ and R = $^{15}N/^{14}N$ for $\delta^{15}N$. Analytical quality was monitored with USGS-62 (measured $\delta^{13}C$ = -14.58 ± 0.18 ‰, $\delta^{15}N$ = +20.16 ± 0.33 ‰, 1SD), which gave good agreement with expected values ($\delta^{13}C$ = –14.79 ± 0.04 ‰, $\delta^{15}N$ = +20.17 ± 0.06 ‰). Replicate analyses on samples yielded a precision of 0.4 ‰ for $\delta^{15}N$ and 0.5 ‰ for $\delta^{13}C$. In addition, we analysed three international iron-oxide reference materials and obtained good reproducibility for those as well (Table S-1). The decarbonated residues were too small to perform nitrogen isotope analyses, but they could be used to measure $\delta^{13}C_{org}$. To our knowledge, these reference materials have not previously been analysed for nitrogen isotopes, prohibiting us from comparing our results to the published literature. But hopefully, our work will stimulate more work on these materials in the future.

We note that the analytical uncertainty for USGS-62 in our measurements is slightly larger than that of the expected value reported by Schimmelmann *et al*. (2016). In their study, this standard was analysed by nine different laboratories, and the reported standard deviation ranges from 0.02 to 0.34 ‰. Hence our measured standard deviation falls within the range of other laboratories. The fact that it is larger than elsewhere does not impact the interpretation of our data as the total range in $\delta^{15}N$ values of the samples is more than one order of magnitude greater than the analytical uncertainty.

To ensure that the measured values are not impacted by the low N-quantities and hence small peak sizes in our samples, we looked at the measured $\delta^{15}N$ values of a series of USGS-41 standards, which were used for calibrating N abundances in the samples (Figure S-1). We find good reproducibility down to peak areas (total integrated peak for both isotopes) of at least 4 Vs, which was the smallest area assessed here. In our sample set, almost all peaks were above 7 Vs and many above 10 Vs, meaning that we have no reason to suspect poor accuracy due to low N abundances. Only two samples produced smaller peaks of 2.5 and 2.8 Vs (SO33-52GTV-1a and SO33-52GTV-2), which explain the slightly larger standard deviations for those, but even those slightly larger uncertainties are still small enough to distinguish those samples from others in the data set.

Lastly, the acid treatment of the samples mobilized carbonate, as well as phosphate and some metal oxides. The total organic carbon content of the residue ($TOC_{residue}$) was corrected for this mass loss to obtain the total organic carbon content of the bulk rock (TOC_{bulk}). To determine the abundance of total inorganic carbon (TIC), we subtracted the calculated TOC_{bulk} concentration from the measured total carbon content of untreated sample (TC). The isotopic composition of inorganic carbon ($\delta^{13}C_{carb}$) was calculated by mass balance, using the abundances and measured values of $\delta^{13}C_{org}$ and $\delta^{13}C_{bulk}$.

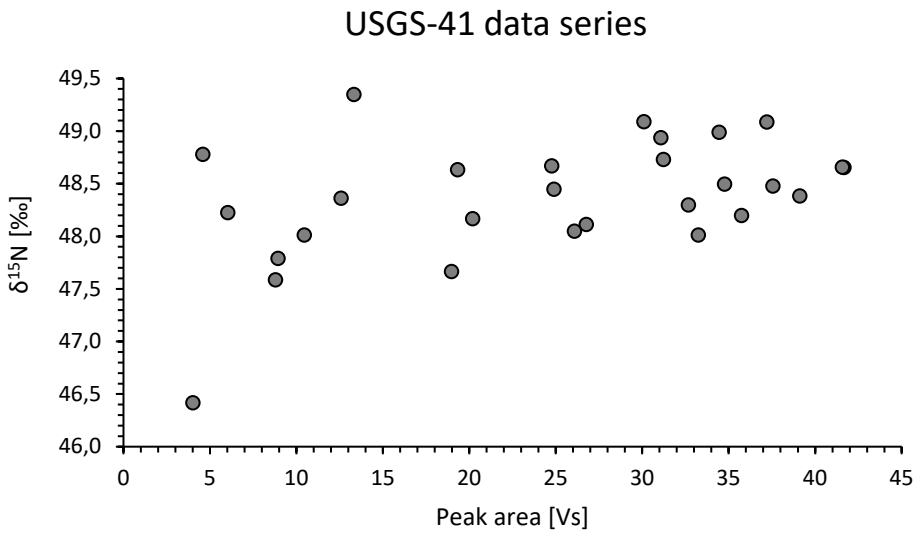

Figure S-1 Series of USGS-41 standards analysed with different masses to test for systematic isotopic bias in small samples. No such bias was found down to peak sizes of at least 4Vs.

Supplementary Table

Table S-1 Analytical results. TN = total nitrogen, TC = total carbon, TOC = total organic carbon, TIC = total inorganic carbon, SD = standard deviation, RE = relative error, HCl loss = fraction of material lost during HCl treatment.

	TN [µg/g]	RE [%]	$\delta^{15}N_{bulk}$ [‰]	SD [‰]	TC [wt. %]	RE [%]	$\delta^{13}C_{bulk}$ [‰]	SD [‰]	HCl loss [wt. %]	$TOC_{resid.}$ [wt. %]	RE [%]	$\delta^{13}C_{org}$ [‰]	SD [‰]	TOC_{bulk} [µg/g]	TIC [µg/g]	$\delta^{13}C_{carb}$ [‰]
Hydrogenetic crusts:																
SO66-500	67	2.1	-6.52	0.49	0.39	1.5	-22.78		97.40	2.87		-27.74		744	3122	-21.60
SO66-503	81	0.8	-7.87	0.13	0.37	2.2	-21.91		97.42	3.45		-27.93		890	2803	-20.00
SO66-506	46	0.8	-4.89	0.05	0.37	2.4	-21.50		98.08	4.86		-27.74		933	2769	-19.40
SO66-507	49	3.4	-9.48	0.69	0.44	1.8	-22.08		98.98							
SO66-513	57	2.5	-12.07	0.34	0.14	2.1	-13.76	0.61	96.12	0.23		-28.60		89	1348	-12.78
SO66-518	62	0.9	1.47	0.05	0.46	4.6	-23.03		99.96	9.15		-27.89		36	4585	-23.00
SO66-522	51	2.6	1.08	0.13	0.22	1.4	-16.04	0.20	98.12	0.56		-28.33		106	2084	-15.42
SO66-524	39	1.8	3.04	0.41	0.31	1.6	-17.40	0.24	98.25	1.31		-28.04		230	2880	-16.54
SO66-526	66	1.7	1.68	0.04	0.17	2.1	-17.92	0.96	100.00							
SO66-531	64	0.1	2.98	0.24	0.29	0.1	-13.41	0.00	89.79	0.27		-26.53		280	2621	-12.01
SO66-545	43	3.2	-3.58	0.95	0.34	3.2	-21.44	1.06	98.76							
Hydrogenetic nodules:																
Chinese Nodule-1a	214	2.6	10.04	0.19	0.18	2.8	-18.00	0.40	59.25	0.07		-23.08		304	1446	-16.93
Chinese Nodule-1b	228	3.2	10.11	0.39	0.17	1.8	-19.11	0.01	56.67	0.07	3.5	-22.89	0.34	290	1452	-18.29
Chinese Nodule-2	173	1.6	12.21	0.07	0.10	5.3	-14.07	0.81	49.21	0.04		-19.43		179	810	-12.88
SO33-52GTV-1a	30	5.0	4.30	1.61	0.16	5.0	-11.89	0.82	68.15	0.04		-22.91		121	1492	-11.26
SO33-52GTV-2	31	3.4	4.51	0.94	0.17	4.7	-13.80	0.88	85.21	0.04		-23.95		53	1647	-13.47
Diagenetic nodules:																
Discol-KD1313	151	7.3	5.14	0.98	0.08	2.6	-19.41	0.26	41.20	0.03		-21.07		192	573	-18.85
SO106-159KG	116	2.4	3.66	0.27	0.28	3.0	-25.84	0.44	31.84	0.13		-25.41		913	1910	-26.04
SO106-159KG-125-180um	118	2.3	2.93	0.60	0.11	4.7	-23.50	0.81	32.10	0.07		-24.89		496	571	-18.20
SO106-163KG-1	164	2.2	6.35	0.38	0.17	0.9	-15.83	1.37	34.58	0.06	6.7	-23.34	0.10	397	1307	-14.26
SO106-163KG-1a	163	0.7	6.44	0.36	0.14	3.0	-15.76	0.29	44.98	0.03		-20.84		166	608	-14.55
SO106-163KG-2	83	0.5	6.13	0.08	0.11	5.4	-14.27	0.77	46.16	0.08		-24.69		436	706	-8.34
SO79-62KD-1a	155	4.6	6.79	0.90	0.11	1.1	-18.51	0.38	37.18	0.03	1.6	-20.36	0.02	162	904	-18.18
SO79-62KD-2	82	5.2	6.98	0.30	0.05	2.2	-18.84	0.45	39.74	0.02	2.6	-20.38	0.28	101	370	-18.49

	TN [µg/g]	RE [%]	$\delta^{15}N_{bulk}$ [‰]	SD [‰]	TC [wt. %]	RE [%]	$\delta^{13}C_{bulk}$ [‰]	SD [‰]	HCl loss [wt. %]	$TOC_{resid.}$ [wt. %]	RE [%]	$\delta^{13}C_{org}$ [‰]	SD [‰]	TOC_{bulk} [µg/g]	TIC [µg/g]	$\delta^{13}C_{carb}$ [‰]
Certified Reference materials (FeMn nodules):																
CRM-JMn-1 (mix hyd+dia)	125	2.4	6.78	0.02	0.12	9.8	-13.82	0.25								
CRM-Nod-A1 (hydrogenetic)	103	9.8	4.33	0.13	0.20	0.1	-7.99	0.16								
CRM-Nod-P1 (mix hyd+dia)	154	1.4	9.13	0.12	0.20	4.9	-7.03	0.50								

Supplementary Information References

Schimmelmann A., Qi H., Coplen T.B., Brand W.A., Fong J., Meier-Augenstein W., Kemp H.F., Toman B., Ackermann A., Assonov S., Aerts-Bijma A.T. (2016) Organic reference materials for hydrogen, carbon, and nitrogen stable isotope-ratio measurements: caffeines, n-alkanes, fatty acid methyl esters, glycines, L-valines, polyethylenes, and oils. *Analytical Chemistry* 88, 4294-4302. https://doi.org/10.1021/acs.analchem.5b04392

Stüeken E.E., de Castro M., Krotz L., Brodie C., Iammarino M., Giazzi G. (2020) Optimized switch-over between CHNS abundance and CNS isotope ratio analyses by Elemental Analyzer-Isotope Ratio Mass Spectrometry: Application to six geological reference materials. *Rapid Communications in Mass Spectrometry*, 34(18):e8821. https://doi:10.1002/rcm.8821